Electronic Supplementary Information

Multilayered Paper-Like Electrodes Composed of Alternating Stacked Mesoporous Mo_2N Nanobelts and Reduced Graphene Oxide for Flexible All-Solid-State Supercapacitors

Guoqiang Ma,[a] Zhe Wang,[a] Biao Gao,[b] Tianpeng Ding,[a] Qize Zhong,[a] Xiang Peng,[c] Jun Su,[a] Bin Hu,[a] Longyan Yuan,[a] Paul K Chu,[c] Jun Zhou[a] and Kaifu Huo*[a]

[a] Wuhan National Laboratory for Optoelectronics (WNLO), School of Optical and Electronic Information, Huazhong University of Science and Technology, Wuhan 430074, China.

[b] The State Key Laboratory of Refractories and Metallurgy, Wuhan University of Science and Technology, Wuhan 430081 (P. R. China),

[c] Department of Physics and Materials Science, City University of Hong Kong,
Kowloon, Hong Kong, China

[*] E-mail: kfhuo@hust.edu.cn

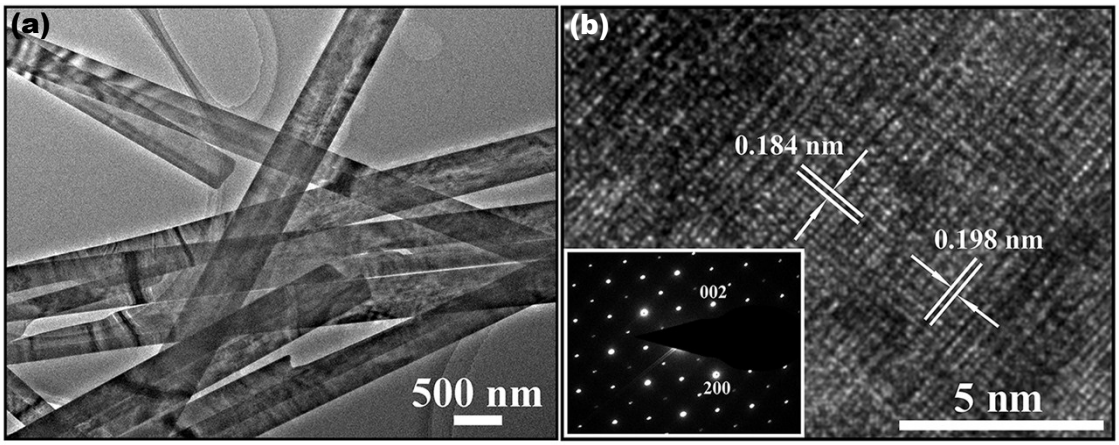

Fig. S1 (a) TEM image of MoO_3 nanobelts. (b) High-resolution TEM image of MoO_3 nanobelts. Inset: corresponding SAED pattern.

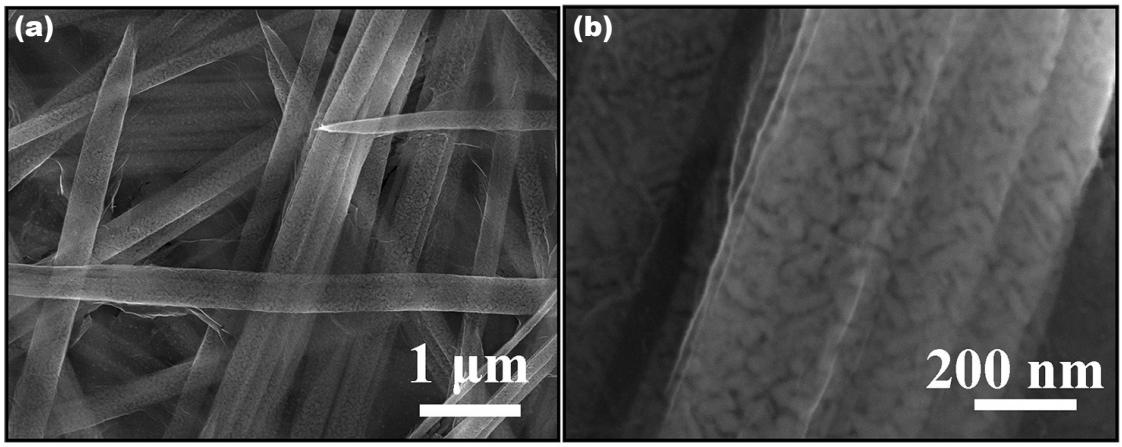

Fig. S2 Top-view SEM images for free-standing MMNNBs/rGO film.

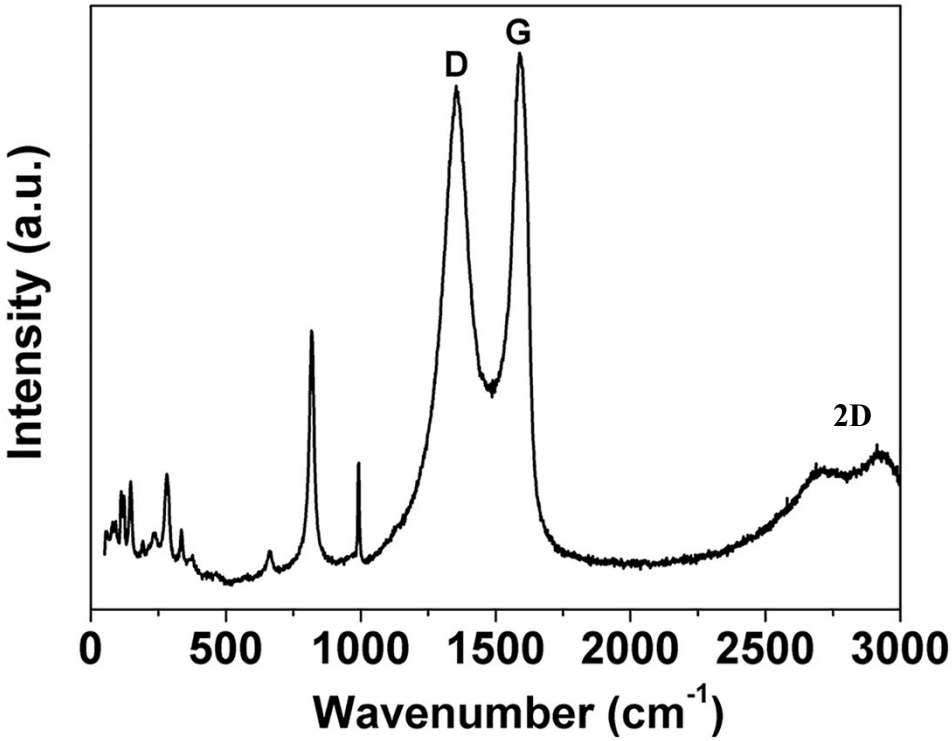

Fig. S3 Raman spectrum for free-standing MMNNBs/rGO film.

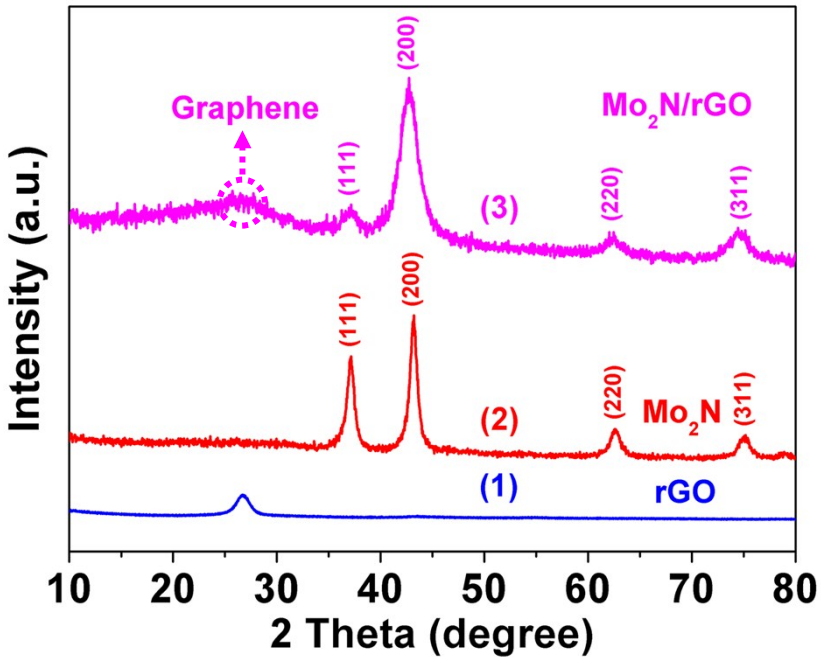

Fig. S4. XRD patterns of rGO, mesoporous Mo_2N nanobelts powder and free-standing mesoporous Mo_2N/rGO film.

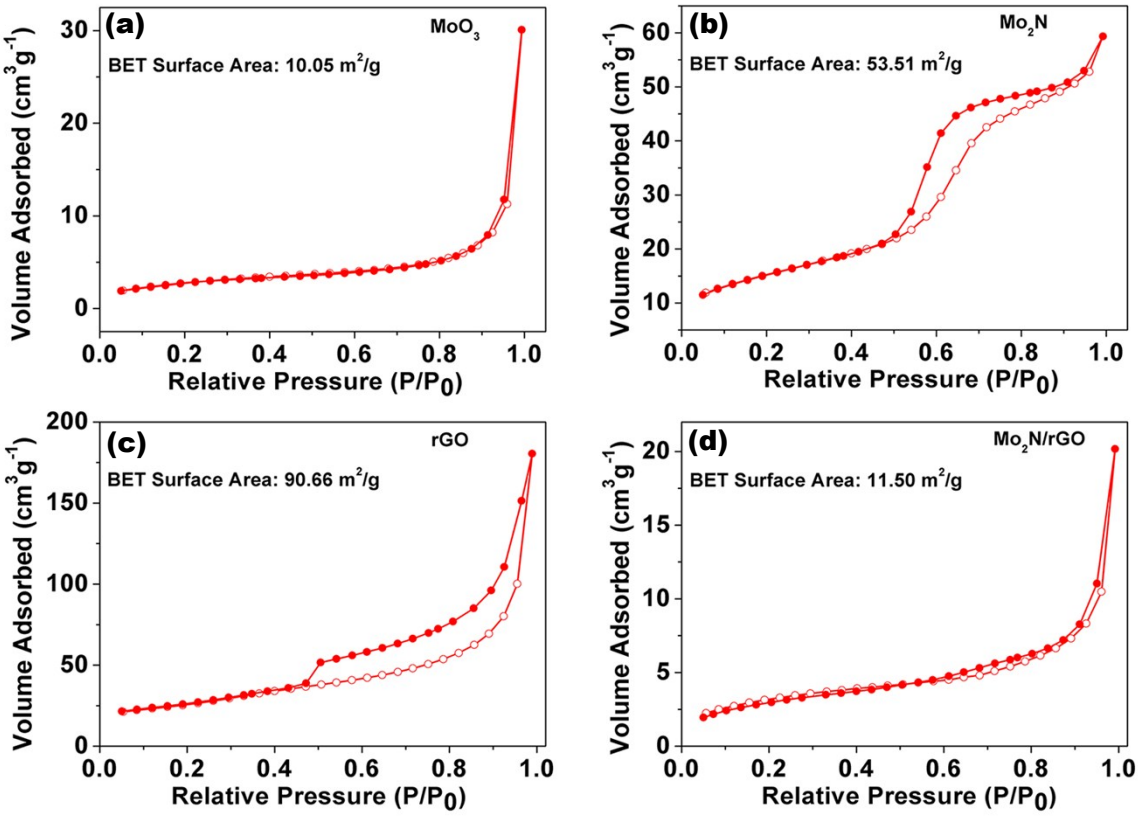

Fig. S5 Nitrogen adsorption-desorption isotherms of MoO_3 (a), Mo_2N (b), rGO (c) and MMNNBs/rGO (d).

Nitrogen adsorption-desorption isotherms were measured under 77K using micromeritics ACAP 2020 analyzer. The specific surface area of the samples was calculated from the N_2 adsorption-desorption isotherms using the Branauer-Emmett-Teller (BET) equation.

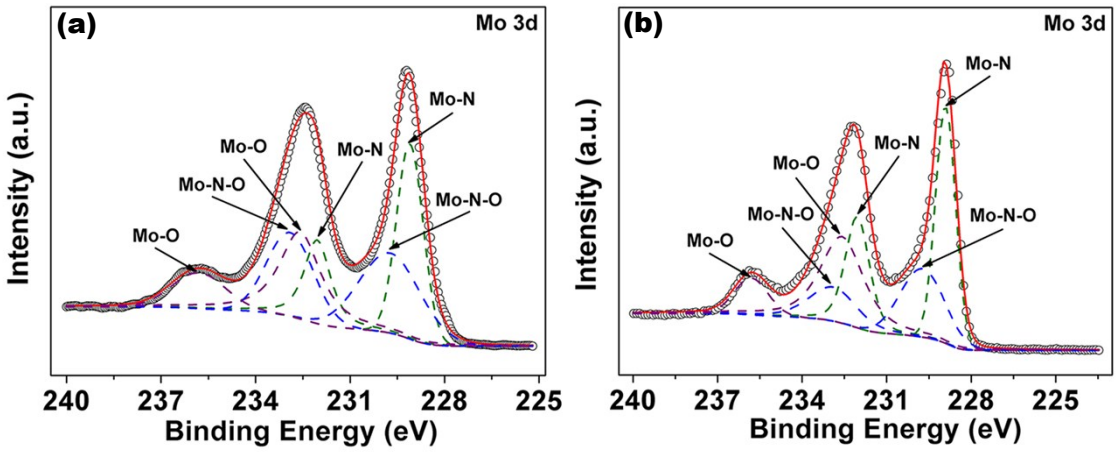

Fig. S6 (a) High-resolution XPS signals of Mo 3d of paper-like free-standing MMNNBs/rGO hybrid film electrode. (b) Core level Mo 3d XPS spectra collected for the Mo_2N nanobelts powder. The Mo 3d exhibits the same three states for free-standing MMNNBs/rGO hybrid film electrode and Mo_2N nanobelts powder, showing the GO has no effect on the nitridation of MoO_3.

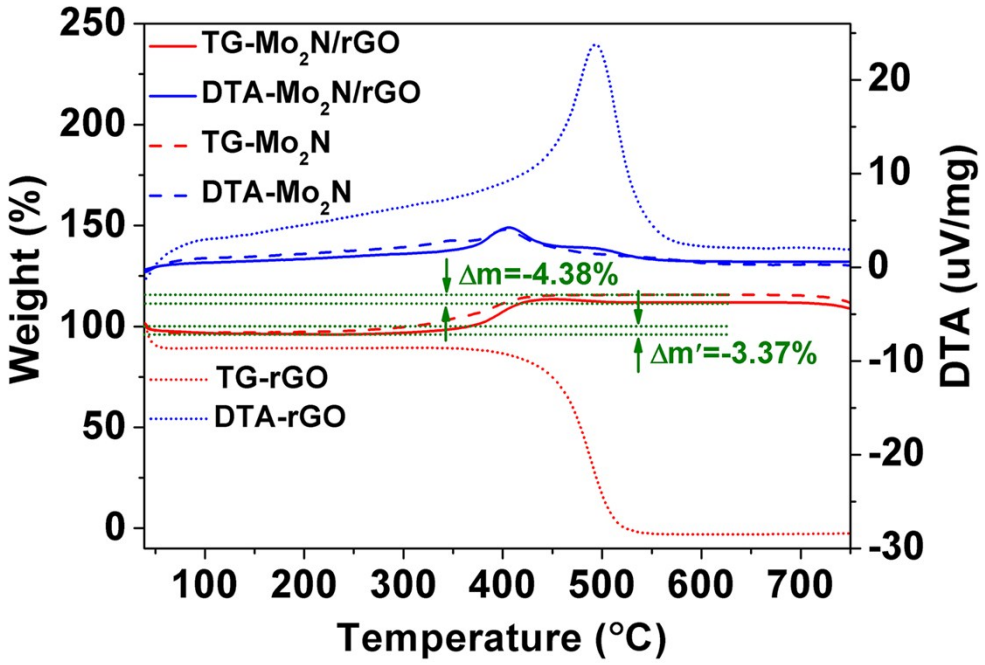

Fig. S7 TG and DTA results for freestanding MMNNBs/rGO hybrid film, mesoporous Mo_2N nanobelts powder and rGO powder.

In order to identify the content of rGO in the free-standing MMNNBs/rGO hybrid film, a combined differential thermal analysis (DTA) and thermogravimetric analysis (TGA) were performed in the air at a heating rate of 5 ^oC min^{-1}. As shown in Fig. S7, the slow weight-loss (Δm=-3.37%) between 39 ^oC and 100 ^oC can be attributed to the loss of the physically adsorbed water. When the temperature was increased to 300 ^oC, the weight of MMNNBs/rGO hybrid film gradually augmented because of the oxidation of Mo_2N, meanwhile, rGO in the composite began to oxidation and decomposition, resulting in a small weight loss for MMNNBs/rGO hybrid film. As a comparison, we also carried out the TGA and DTA tests for rGO and Mo_2N. As indicated in Fig. S7, the significant weight loss in the rGO TG curve and the corresponding exothermal peak on the DTA curve between 400 ^oC and 550 ^oC can be indexed to the combustion of rGO. Similarly, the significant weight increment displayed on the Mo_2N TG curve and the corresponding exothermal peak on the DTA curve between 370 ^oC and 440 ^oC are associated with the oxidation of Mo_2N to MoO_3. Based on the above analysis, the content of rGO in the free-standing MMNNBs/rGO hybrid film can be determined to be 4.38%.

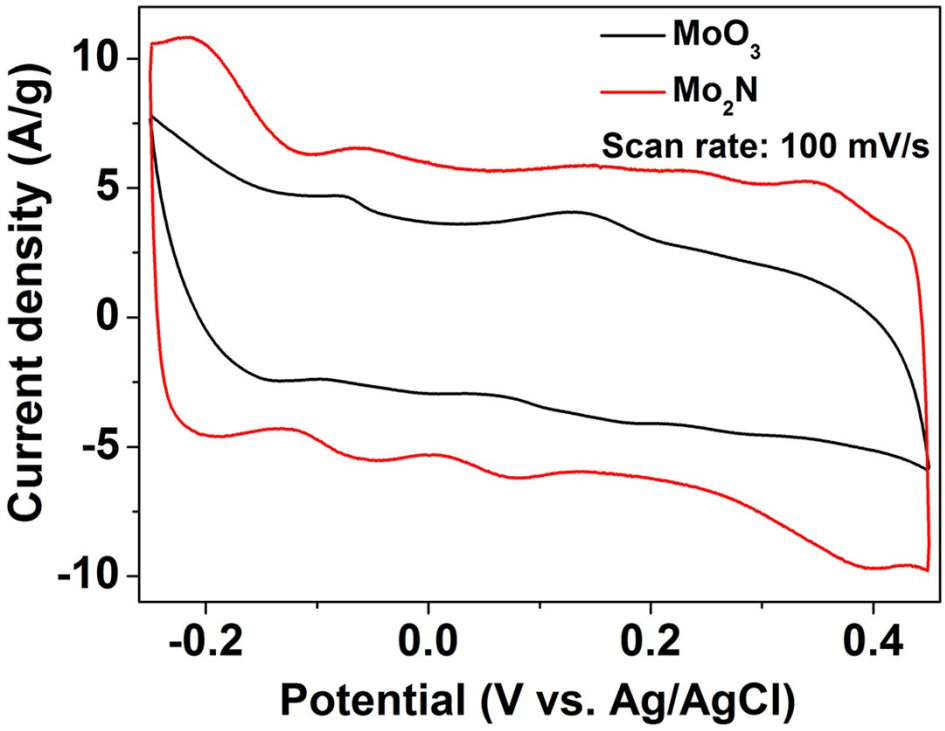

Fig. S8 Comparison of CV curves for MoO_3 and Mo_2N in the 1M H_2SO_4 aqueous electrolyte at 100 mV/s.

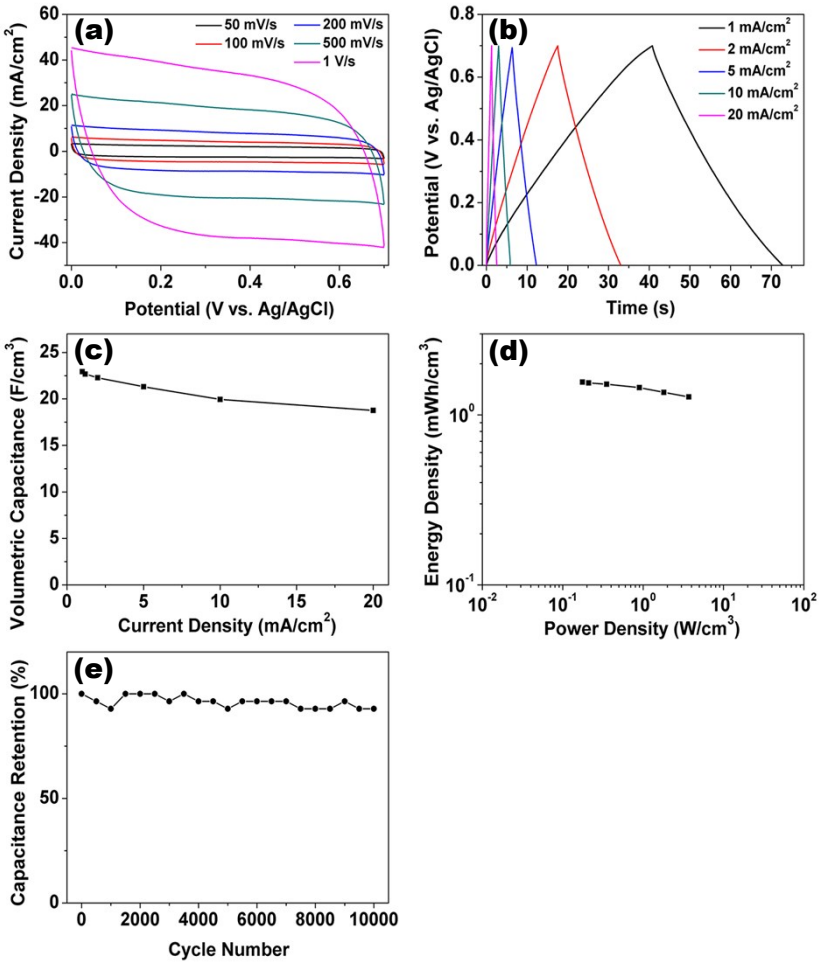

Fig. S9 Electrochemical performances for MMNNBs/rGO based symmetrical devices by a coin-cell configuration. (a) CV curves at different san rates. (b) Galvanostatic charge-discharge curves at different current densities. (c) Volumetric capacitance as a function of current density. (d) Ragone plot. (e) Cycle life.

We assembled a symmetrical SC (SSC) device using a two-electrode coin cell configuration with 1M aqueous H_2SO_4 as an electrolyte. Specifically, two pieces of paper-like free-standing MMNNBs/rGO hybrid electrodes with the diameter of 0.8 cm, one piece of separator, and 1M H_2SO_4 were used as electrodes, separator and electrolyte, respectively. And the all electrochemical tests were performed at room temperature. As shown in Fig. S9a, the SSC device can be operated in the potential window range of 0-0.7 V under various scan rates ranging from 5 mV s^{-1} to 1 V s^{-1}. It can be seen that the CV curves retained the quasi-rectangular shape, characteristic of ideal electrochemical electric double layer capacitive behavior, even at the san rate up to 1 V s^{-1}, indicating the superior electrochemical charge storage properties of the SSC device as well as the ultrafast response of the electrodes. Fig. S9b showed the GCD curves for SSC device with the current densities increased from 1 mA cm^{-2} to 20 mA cm^{-2}. The linear and symmetric curves further indicated the ideal capacitive

performance and rapid charge/discharge characteristic of the SSC device based on paper-like free-standing MMNNBs/rGO hybrid electrodes. The corresponding volumetric capacitance as a function of current density was plotted in Fig. S9c. The volumetric capacitance based on the electrode was 22.93 F cm^{-3} at the current density of 1 mA cm^{-2} (corresponding to 0.5 A cm^{-3}), which was substantially higher than the values reported in the literatures, such as carbon/MnO_2 based SCs 0.177 F cm^{-3},[ref. 6] graphene-based SCs 0.45 F cm^{-3},[ref. 7] and H-TiO_2@MnO_2//H-TiO_2@C core-shell asymmetric SCs 0.9 F cm^{-3}.[ref. 8] Furthermore, the SSC device exhibited excellent rate capability with the specific capacitance remaining at 82% when the current density was increased 20 fold from 1 mA cm^{-2} to 20 mA cm^{-2}. Fig. S9d showed the Ragone plot of the SSC device based on paper-like free-standing MMNNBs/rGO hybrid electrodes, from which the highest volumetric energy density of 1.56 mWh cm^{-3} was obtained at a power density of 0.18 W cm^{-3}, and the highest volumetric power density of 3.71 W cm^{-3} at a energy density of 1.28 mWh cm^{-3}, respectively. Remarkably, the maximum volumetric energy density obtained here was evidently superior to the reported values.[6, 8] As practical application for energy storage system, the cycle life is also an especially important factor for electrochemical SC. As shown in Fig. S9e, after 10 000 cycles, the capacitance retention of the SSC device can still maintain 93%.

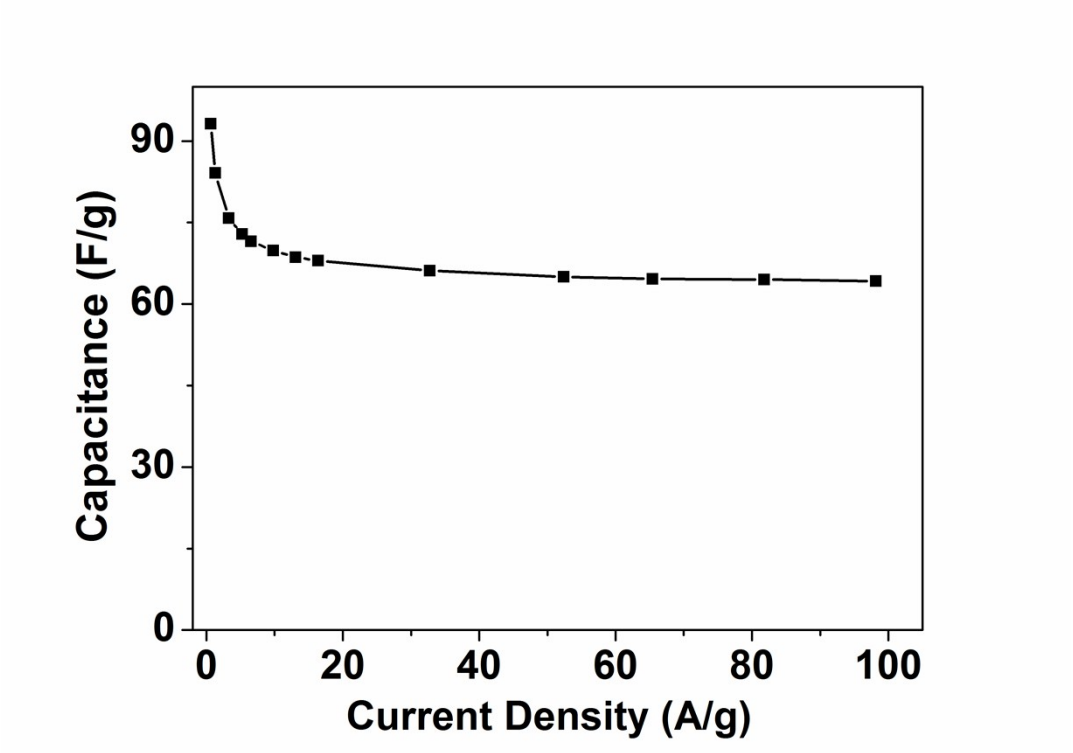

Fig. S10 Gravimetric capacitance of the freestanding MMNNBs/rGO hybrid film electrode as a function of current density.

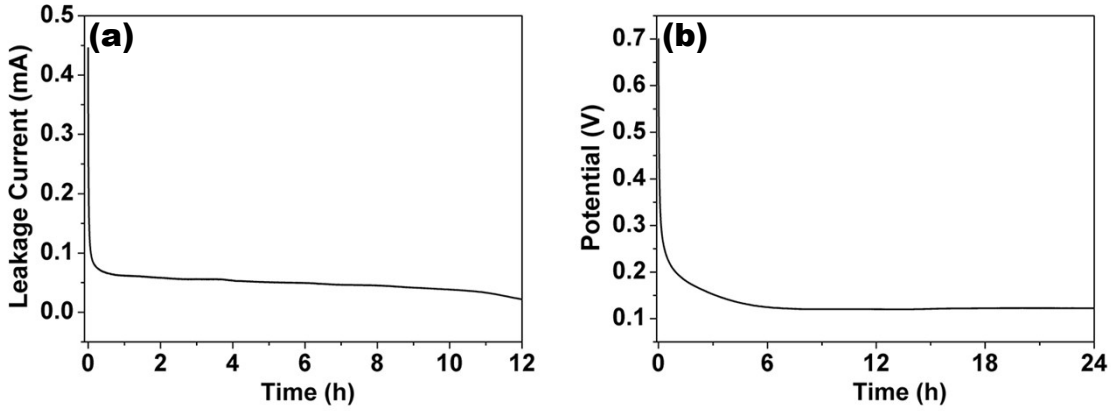

Fig. S11 Leakage current (a) and self-discharge (b) curves for the all-solid-state device.

Table S1. Comparison of gravimetric capacitance for other active materials

Active materials	Capacitance	Electrolyte	Ref.
NbN	73 F/g at 2 mV/s	KOH	[1]
WN	30 F/g at 2 mV/s	KOH	[2]
γ-W_2C	79 F/g at 2 mV/s	H_2SO_4	[3]
PANI/SWCNT film	55 F/g at 2.6 A/g	H_2SO_4	[4]
Mesoporous carbon sphere arrays	84 F/g at 0.1 A/g	$(C_2H_5)_4NBF_4$/PC	[5]
MMNNBs/rGO	93.2 F/g at 0.7 A/g	H_2SO_4	Our Work
	64.2 F/g at 98.2 A/g		

References:

1 D. Choi, P. N. Kumta, *J. Am. Ceram. Soc.,*, 2011, **94**, 2371.

2 D. Choi, P. N. Kumta, *J. Am. Ceram. Soc.,*, 2007, **90**, 3113.

3 J. Ge, G. Cheng, L. Chen, *Nanoscale*, 2011, **3**, 3084.

4 H. -J. Liu, W. -J. Cui, L. -H. Jin, C. -X. Wang, Y. -Y. Xia, *J. Mater. Chem.*, 2009, **19**, 3661.

5 P. Pande, P. G. Rasmussen, L. T. Thompson, *J. Power Sources*, 2012, **207**, 212.

6 Q. Li, X. -F. Lu, H. Xu, Y. -X. Tong, G. -R. Li, *Acs Appl. Mater. Interfaces*, 2014, **6**, 2726.

7 M. F. El-Kady, V. Strong, S. Dubin, R. B. Kaner, *Science*, 2012, **335,** 1326.

8 X. Lu, M. Yu, G. Wang, T. Zhai, S. Xie, Y. Ling, Y. Tong, Y. Li, *Adv. Mater.*, 2013, **25**, 267.